



*J. Serb. Chem. Soc.* 85 (6) 765–779 (2020)  
JSCS-5337

# Journal of the Serbian Chemical Society

JSCS-info@shd.org.rs • www.shd.org.rs/JSCS

UDC 547.786+547.821.411.3'551.41:

66.095.252.091.7:538.913

*Original scientific paper*

## Understanding the regio- and diastereoselective synthesis of a potent antinociceptive isoxazolidine from C-(pyridin-3-yl)-N-phenylnitrone in the light of molecular electron density theory

NIVEDITA ACHARJEE\*

Department of Chemistry, Durgapur Government College, J.N. Avenue, Durgapur-713214,  
West Bengal, India

(Received 14 September, revised 19 November, accepted 16 December 2019)

**Abstract:** [3+2] cycloaddition reaction of *C*-(pyridin-3-yl)-*N*-phenylnitrone and 2-propen-1-ol yields stereochemically defined potent antinociceptive isoxazolidine derivative. Computational quantum calculations (CQC) are performed for this synthesis to predict the polar character, mechanism and selectivity within the framework of molecular electron density theory (MEDT). Topological analysis of the electron localization function (ELF) classifies the nitrone as a zwitter-ionic(zw-) type three atom component (TAC) showing absence of any pseudoradical or carbenoid centre. Four reaction channels corresponding to the possible regio- and stereoselective pathways are studied at DFT/B3LYP/6-311G(d,p) level of theory. The reaction follows one-step mechanism with asynchronous transition states and the computed activation energies agree well with experimental data. The reaction can be differentiated into nine ELF topological phases, with faster C–C bond formation. Global electron density theory (GEDT) at the favoured transition state and conceptual density functional theory (CDFT) indices at the ground state of the reagents indicate non-polar character. Non-covalent interactions are predicted by atoms-in-molecules (AIM) analysis and non-covalent interaction (NCI) plots at the transition states.

**Keywords:** MEDT; transition state; electron localization function; NCI.

### INTRODUCTION

Isoxazolidine moiety forms the core of several biologically active compounds showing antibacterial, antiviral, anticancer and anti-inflammatory activities<sup>1</sup>. Structure and stereochemistry of a drug plays a decisive role in its biological activity. Thus, synthesis of a biologically active compound should involve proper regio- and stereochemical control to yield the target isomer. This control

\* E-mail: nivchem@gmail.com  
<https://doi.org/10.2298/JSC190914136A>

is the outcome of lowered activation energy barrier along the favored approach mode, leading to feasibility of the targeted synthesis. [3+2] cycloaddition reactions<sup>2</sup> (32CA) remain a versatile protocol for the regio- and stereochemical synthesis of isoxazolidine systems.

Molecular electron density theory<sup>3</sup> (MEDT) proposed by Domingo in 2016 states that change in electron density is responsible for molecular reactivity in organic reactions. This theory has been widely illustrated for 32CA reactions<sup>4–6</sup> as well as for other processes, for which one-step “pericyclic mechanism” has been earlier postulated such as Diels–Alder reactions,<sup>7,8</sup> thermal elimination reaction,<sup>9,10</sup> [3,3] sigmatropic shifts,<sup>11</sup> etc. Initially, topological analysis of the electron localisation function<sup>12</sup> (ELF) and detailed analysis of conceptual density function theory (CDFT) indices<sup>13</sup> at the ground state of the reagents is performed within MEDT. The ELF concept<sup>12,14</sup> provides an appealing procedure to establish a straightforward connection between the chemical structure and electron density distribution in molecular systems. Core basins are associated with the nuclei. Monosynaptic basins, denoted by V(A), are associated with non-bonding regions (lone pairs and pseudoradical centers) and disynaptic regions, denoted by V(A,B) are associated with the bonding region between A and B. ELF valence basin populations can be used to recover the Lewis bonding model and provide a reasonably suggestive chemical representation of the molecular system. Topological analysis of the ELF and visualization of ELF localisation domains has been employed in several MEDT studies<sup>4–6</sup> to analyse the reactivity of three-atom components<sup>4–6</sup> (TACs) participating in 32CAs. This has allowed the classification of TACs into pseudodiradical (pdr-)<sup>15</sup> type, pseudo(mono)radical<sup>16</sup> (pmr-) type, carbenoid (cb-)<sup>15</sup> type and zwitter-ionic (zw-)<sup>5,6,17</sup> type. Monosynaptic V(A) basin integrating at a population of less than 1e is associated with pseudoradical center, while that integrating at a population of 2e in neutral molecules is associated with carbenoid centre. TACs with one pseudoradical center are classified as pmr- type, with two pseudoradical centers as pdr- type and with a carbenoid centre as cb- type. The activation energies of TACs follows the order,<sup>6</sup> pdr-type<pmr-type≈cb-type<zw-type.

Detailed exploration of the potential energy surface (PES) associated with all possible approach modes is done to study the energy profile, followed by calculation of global electronic flux at the transition states in terms of global electron density transfer (GEDT)<sup>18</sup> to predict the polar character. GEDT is calculated by the natural bond orbital analysis<sup>19,20</sup> of the two reacting frameworks at the most favourable transition state. GEDT values less than 0.2e are associated with non-polar reactions, while polar<sup>21</sup> processes are associated with GEDT values higher than 0.2e.<sup>18,21</sup>

The topological analysis of the ELF along the intrinsic reaction coordinate (IRC)<sup>22</sup> pathway, is done to analyze the complete reaction course with a clear

idea of the bond-breaking and bond making processes (bonding evolution theory (BET) <sup>23,24</sup> study). Finally, the covalent/non-covalent interactions at the interatomic bonding regions are analysed by the calculation of quantum theory of atoms in molecules (QTAIM)<sup>25,26</sup> parameters and visualization of non-covalent interaction (NCI)<sup>27</sup> gradient isosurfaces.

The present investigation reports MEDT study at DFT/B3LYP/6-311G(d,p) level for the synthesis of a regio- and stereochemically defined isoxazolidine nicotine analogue from [3+2] cycloaddition reaction of C-(pyridin-3-yl)-N-phenylnitrone to 2-propen-1-ol. This biologically active cycloadduct was synthesized in 2014<sup>1,28</sup> and shows potent antinociceptive properties, greater efficacy than pentazocine and high tolerability. It is safer than nicotine for mitigation of analgesic states. The present investigation aims to present a complete theoretical rationalization for the synthesis. The study has been divided into five sections: 1) topological analysis of the ELF at the ground state of the reagents, 2) analysis of CDFT indices, 3) location of transition states along all possible approach modes, study of the energy profile and GEDT, 4) ELF topological analysis along the IRC pathway of the favoured transition state and 5) study of the interactions at the interatomic bonding region by QTAIM and NCI studies.

#### COMPUTATIONAL METHODS

Density functional theory (DFT) calculations were carried out using B3LYP functional<sup>29,30</sup> in conjunction with the 6-311G(d,p) basis set. The optimized geometries were then characterized at the same level to ensure that the reactants and products do not have any imaginary frequency and the transition states have one and only one imaginary frequency. The intrinsic reaction coordinate (IRC) pathways of the investigated CAs were traced using the second order Gonzales–Schlegel integration method.<sup>22</sup> The global electron density transfer (GEDT<sup>18</sup>) was computed by the sum of the natural atomic charges ( $q$ ), obtained by a natural population analysis (NPA).<sup>19,20</sup> Conceptual DFT (CDFT) global reactivity indices,<sup>13,31</sup> i.e., electronic chemical potential ( $\mu$ ),<sup>32</sup> global hardness ( $\eta$ )<sup>33</sup> and global electrophilicity ( $\omega$ )<sup>34</sup> and nucleophilicity index ( $N$ )<sup>35</sup> are calculated as proposed in the literature.<sup>13</sup> Solvent effects in toluene were taken into account by optimization of the stationary states using conductor like polarizable continuum model (PCM).<sup>36,37</sup> Thermodynamic parameters were calculated in toluene at 383 K (refluxing toluene temperature). Computational studies were performed using Gaussian 03 suite of programs (revision D.01).<sup>38</sup> ELF topological studies and calculation of QTAIM parameters was performed using Multiwfn<sup>39</sup> program. Non-covalent interactions<sup>22</sup> (NCIs) were analyzed through evaluation of the B3LYP/6-311G(d,p) mono-detrimental wave functions of the located transition states by using Multiwfn program.<sup>39</sup> ELF basin analysis was performed with high quality grid with spacing 0.06 Bohr. ELF attractor images were visualized using VMD software<sup>40</sup> and UCSF Chimera software.<sup>41</sup>

#### RESULTS AND DISCUSSION

##### *ELF topological analysis at the ground state of the reagents*

ELF localization domains, basin attractor positions and the most significant valence basin populations of the reactants **1** and **2** are shown in Fig. 1, with their

proposed Lewis like structures represented in Fig. 2. Topological analysis of the ELF of nitrone **1** shows the presence of two disynaptic basins,  $V(C_3,N_2)$  and  $V(N_2,O_1)$ , integrating total population of  $3.73e$  and  $1.38e$ , respectively, which can be associated with the underpopulated C3-N2 double bond and N2-O1 single bond.

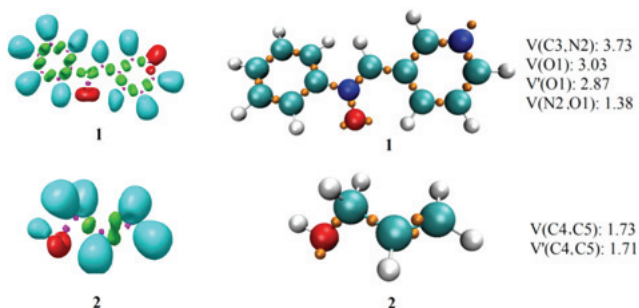


Fig. 1. B3LYP/6-311G(d,p) calculated ELF localization domains (isovalue: 0.80) and basin attractor positions together with the most significant ELF valence basin populations for the reactant molecules **1** and **2**. ELF valence basin population are given in average number of electrons.

Two  $V(O_1)$  and  $V'(O_1)$  monosynaptic basins integrating a total population of  $5.90e$  can be associated with the lone-pair electron density of O1 oxygen. Absence of any pseudoradical centre (monosynaptic basin with total integrating population less than  $1e$ ) or carbeneoid centre (monosynaptic basin with total integrating population of  $2e$  in neutral molecules), instead a C3–N2 double bond in nitrone **1** indicates its zwitter-ionic electronic structure and hence its participation in zw-type 32CAs only, which are associated with high energy barriers. This was evident from the calculated activation parameters (see later). After establishment of the bonding pattern, the charge distribution was analyzed for **1** and **2** through natural population analysis (NPA).<sup>19,20</sup> O1 of **1** is negatively charged by  $-0.53e$  (see Fig. 2), while N2 nitrogen and C3 carbon atoms show negligible charges of  $0.01e$  and  $0.09e$ , respectively (see Fig. 2).

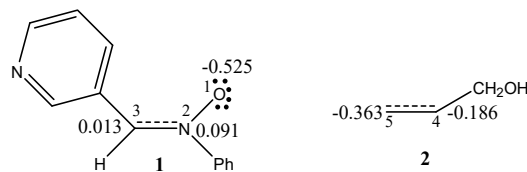


Fig. 2. Proposed Lewis-like structure of reactants (based on ELF basin populations) and calculated natural atomic charges are given in average number of electrons e.

This natural charge framework and the calculated dipole moment  $2.97\text{ D}$  indicates a charge separation in this TAC, making it a dipolar species. However,

the charge separation is not as expected from Lewis bonding model. Thus, the observed charge distribution results from the asymmetric electron density delocalization, which arises due to the presence of different nuclei in a molecular system and not as a consequence of the resonance Lewis structure. ELF topological analysis of olefin **2** shows the presence of two V(C4,C5) and V'(C4,C5) disynaptic basins integrating a total population of 3.44e, which can be associated with an underpopulated C4–C5 double bond. C5 shows greater negative charge compared to C4 (see Fig. 2), which accounts for the influence of hydroxymethyl substituent in 2-propen-1-ol.

#### *Analysis of CDFT indices*

DFT based reactivity indices have been employed to understand the reactivity of chemical reactions in several studies.<sup>13</sup> Thus, these indices (listed in Table I) are computed and analyzed at the ground state of the reagents. CDFT indices of **1**, *C*-(pyridin-2-yl)-*N*-phenylnitrone and *C*-(pyridin-4-yl)-*N*-phenylnitrone slightly differ from each other, which suggests that the position of pyridine nitrogen in the *C*-aryl substituent induces no changes in the global indices. The electronic chemical potential,  $\mu$  of nitrone **1** ( $\mu = -4.07$  eV) shows minimal difference from that of **2** ( $\mu = -3.58$  eV) indicating negligible transfer of electron density. This is also indicated by the calculated GEDT at the most favourable transition state (see later), suggesting a non-polar character. The electrophilicity index,  $\omega$ , value of **1** classifies it as a strong electrophile ( $\omega > 1.50$  eV) within the electrophilicity scale,<sup>34</sup> while **2** is classified as moderate electrophile with  $0.80 \text{ eV} < \omega < 1.50 \text{ eV}$ . **1** is classified as a strong nucleophile<sup>35</sup> with  $N > 3$  eV, while **2** as a moderate nucleophile.

TABLE I. B3LYP/6-311G(d,p) calculated electronic chemical potentials ( $\mu$ ), chemical hardness ( $\eta$ ), electrophilicity ( $\omega$ ) and nucleophilicity ( $N$ )

Reactant	$\mu / \text{eV}$	$\eta / \text{eV}$	$\omega / \text{eV}$	$N / \text{eV}$
<b>1</b>	-4.07	3.84	2.16	3.37
<i>C</i> -(Pyridin-2-yl)- <i>N</i> -phenylnitrone	-4.05	3.86	2.13	3.37
<i>C</i> -(Pyridin-4-yl)- <i>N</i> -phenylnitrone	-4.26	3.89	2.33	3.16
<b>2</b>	-3.58	7.16	0.89	2.20

#### *Study of the energy profile associated with the 32CA between **1** and **2***

32CA reaction between **1** and **2** involves two possible regioisomeric reaction paths, labeled, ortho and meta, associated respectively with the formation of O1–C4 and O1–C5 bonds of the isoxazolidine system (see Fig. 3). Two diastereofacial isomeric reaction paths, labeled endo and exo are associated with these two reaction paths, thus allowing the search for stationary points along these four possible approach modes. This allowed the location and characterization of four TSs, denoted by **TSox**, **TSon**, **TSmx** and **TSmn**, associated respectively with the

ortho/exo, ortho/endo, meta/exo and meta/endo pathways and the corresponding cycloadducts, denoted by **CAox**, **CAon**, **CAmx** and **CAmn**. This 32CA follows one-step mechanism. For each pathway, pre-reaction molecular complexes were formed in the first reaction stage, before the formation of TS. Such molecular complexes have been recently detected for 32CAs of disubstituted nitrones.<sup>42–44</sup> The molecular complexes (MCs) for present study were found to be enthalpic in nature with  $\Delta H$  values of  $-6.7$ ,  $-7.4$ ,  $-4.0$  and  $-1.5$  kcal $^*$  mol $^{-1}$  in gas phase and  $-0.1$ ,  $-0.8$ ,  $-1.8$  and  $-0.4$  kcal mol $^{-1}$  in toluene for **MCox**, **MCon**, **MCmx** and **MCmn**, respectively, relative to the isolated reactants.

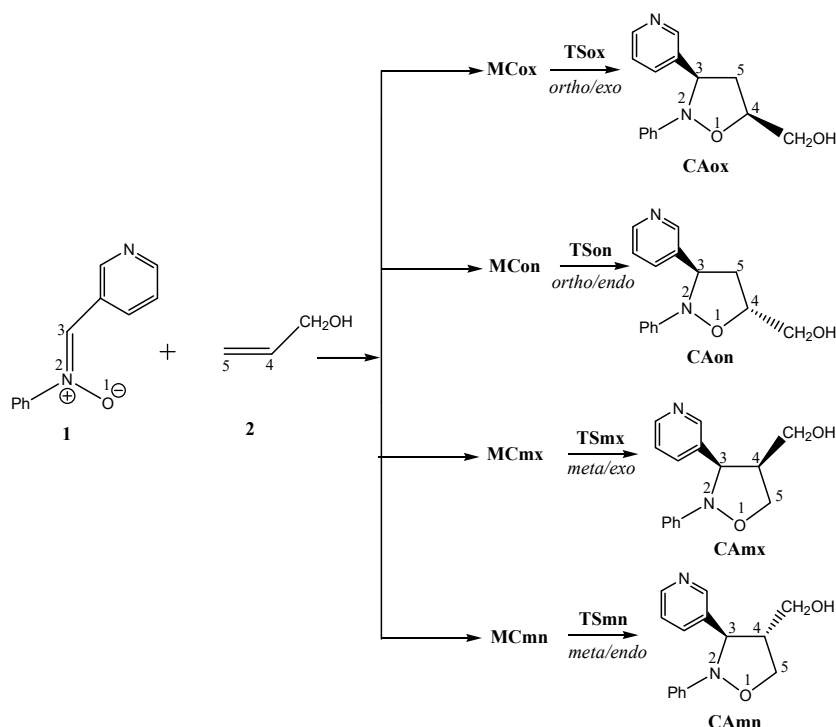


Fig. 3. Possible regio- and stereochemical pathways for the 32CA reaction between **1** and **2**.

The gas phase activation energy of **TSox** is lower than that of **TSon**, **TSmx** and **TSmn** by  $1.5$ ,  $0.8$  and  $2.3$  kcal mol $^{-1}$ . Inclusion of solvent effects in toluene amounts these differences to  $1.6$ ,  $1.4$  and  $2.4$  kcal mol $^{-1}$ , respectively. Thus, the computed activation energies account for the experimentally observed<sup>1</sup>  $75\%$  yield of **CAox** in toluene.<sup>1</sup> The reaction is exothermic with  $\Delta H$  values in the range from  $-13.7$  to  $-16.5$  kcal mol $^{-1}$  in gas phase and from  $-12.3$  to  $-15.1$  kcal mol $^{-1}$  in refluxing toluene (383 K, see Table II). The activation enthalpy of **TSox**

\*  $1$  kcal =  $4184$  J

is less than that of **TSon**, **TSmx** and **TSmn** by 1.5, 0.7 and 2.2 kcal mol<sup>-1</sup> in gas phase and 1.5, 1.4 and 2.3 kcal mol<sup>-1</sup> in toluene (383 K), respectively (see Table II). Inclusion of entropies to enthalpies change strongly increases the activation Gibbs energies change by 13.4–14.3 kcal mol<sup>-1</sup> in gas phase and 17.2–18.3 kcal mol<sup>-1</sup> in toluene, and strongly decreases the reaction Gibbs energies change by 13.5–14.3 kcal mol<sup>-1</sup> in gas phase and 17.4–18.3 kcal mol<sup>-1</sup> in toluene due to the unfavourable entropies associated.  $\Delta G$  of **TSox** becomes 32.0 kcal mol<sup>-1</sup> in gas phase and is less than that of **TSon**, **TSmx** and **TSmn** by 1.5, 1.6 and 2.4 kcal mol<sup>-1</sup>, while  $\Delta G$  of **TSox** becomes 37.2 kcal mol<sup>-1</sup> in refluxing toluene temperature (383 K) and is less than that of **TSon**, **TSmx** and **TSmn** by 1.6, 2.5 and 2.5 kcal mol<sup>-1</sup> predicting formation of ortho/exo adduct as the kinetically controlled product. These activation parameters suggest that this 32CA is regio- and stereoselective, but not regio- and stereospecific. The reaction is kinetically controlled and the reaction channels other than the favored ortho/exo mode are not forbidden from kinetic point of view. Complete regio- and stereoselective 32CA is only possible in case of strong electron withdrawing activation of the ethylene derivative and unequivalent screening of reaction centers in the nitrone molecule. Experimental studies of such fully regio- and stereoselective 32CAs have been recently reported by Jasiński *et al.*<sup>45,46</sup>

TABLE II. B3LYP/6-311G(d,p) calculated  $\Delta E$ ,  $\Delta H$ ,  $\Delta G$  and  $\Delta S$  of products and transition states

TS	$\Delta E$ / kcal mol <sup>-1</sup>		$\Delta H$ / kcal mol <sup>-1</sup>		$\Delta S$ / cal mol <sup>-1</sup> K <sup>-1</sup>		$\Delta G$ / kcal mol <sup>-1</sup>	
	Gas	Toluene	Gas	Toluene	Gas	Toluene	Gas	Toluene
<b>CAox</b>	-19.5	-18.1	-16.5	-15.1	-45.4	-45.4	-3.0	2.3
<b>TSox</b>	17.8	19.1	18.6	20.0	-44.9	-44.8	32.0	37.2
<b>CAon</b>	-19.2	-17.8	-16.2	-14.8	-46.5	-46.4	-2.4	3.0
<b>TSon</b>	19.3	20.7	20.1	21.5	-45.2	-45.0	33.5	38.8
<b>CAmx</b>	-16.9	-15.5	-13.7	-12.3	-47.9	-47.8	0.6	6.0
<b>TSmx</b>	18.6	20.5	19.3	21.4	-47.9	-47.9	33.6	39.7
<b>CAMn</b>	-18.0	-16.6	-14.9	-13.5	-46.8	-46.8	-1.0	4.4
<b>TSmn</b>	20.1	21.5	20.8	22.3	-45.5	-45.3	34.4	39.7

The optimized gas phase geometries of four TSs are given in Fig. 4. At the ortho TSs, the lengths of O1-C4 and C3-C5 forming bonds are 2.14 and 2.15 Å at **TSox** and 2.18 and 2.13 Å at **TSon**, which suggests very low asynchronicity in the bond formation process. This is also indicated by the ELF topological study (see later), when the O1–C4 and C3–C5 bond formation takes place within a short interval along the IRC coordinate. These forming bond distances in the range 2.08–2.18 Å indicate that the formation of two new O1–C4 and C3–C5 single bonds has not yet begun in any of these TSs. This was also evident from the ELF topological analysis and calculated QTAIM parameters (see later). Finally, the polar nature of this 32CA reaction was analyzed by GEDT calcul-

ations at the TSs. Reactions with GEDT value of 0.0e are non-polar, while GEDT values higher than 0.2e are associated with polar processes. For this 32CA, GEDT values of 0.07e-0.08e at the TSs imply a non-polar character, which is in complete agreement with the minimal differences of electronic chemical potentials at the ground state of the reagents (see Table I).

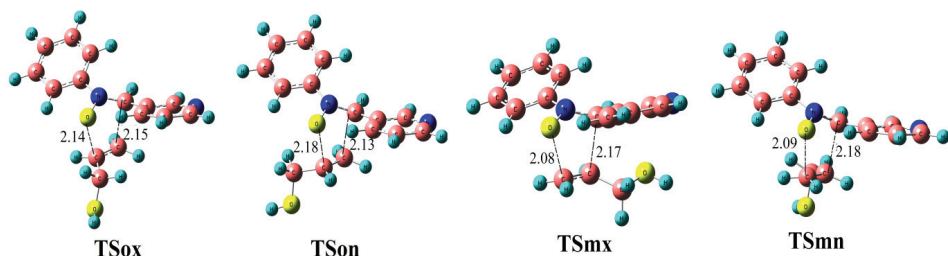


Fig. 4. B3LYP/6-311G(d,p) optimized gas phase transition states.

#### *ELF topological analysis of the C–C and C–O bond formation processes*

The C–C and C–O bond formation processes were characterized by ELF topological analysis along the IRC pathway of the most favourable ortho/exo reaction mode to identify the structures directly involved in the bond formation process. ELF basin populations at the most relevant IRC points are given in Fig. 5.

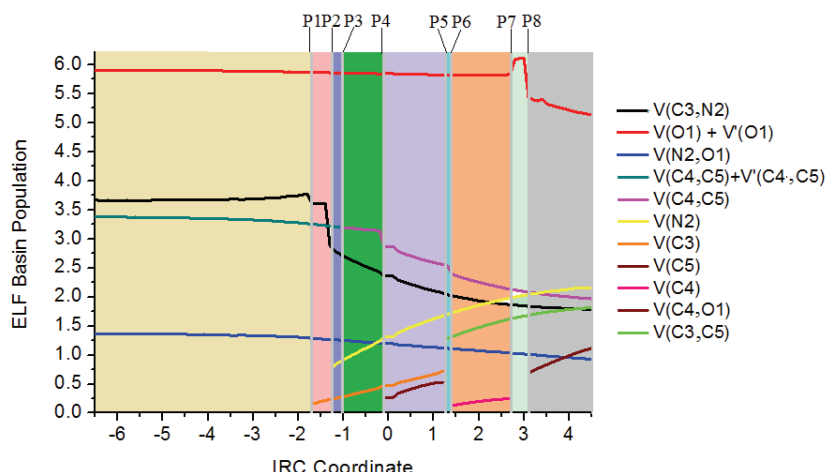


Fig. 5. ELF basin populations of selected IRC points along the favored exo/ortho pathway for 32CA reaction between **1** and **2**.

Some appealing conclusions can be drawn from this ELF study:

1. 32CA reaction between *C*-(pyridin-3-yl)-*N*-phenyl nitrone (**1**) and olefin **2** can be divided into nine phases (Fig. 5) on the basis of calculated ELF basin

populations. Eight IRC points denoted by P1, P2, P3, P4, P5, P6, P7 and P8 are identified to mark the genesis of a new phase along the reaction pathway (see Fig. 5). The basin attractor positions at these points with most significant valence basin populations at these points are shown in Fig. 6.

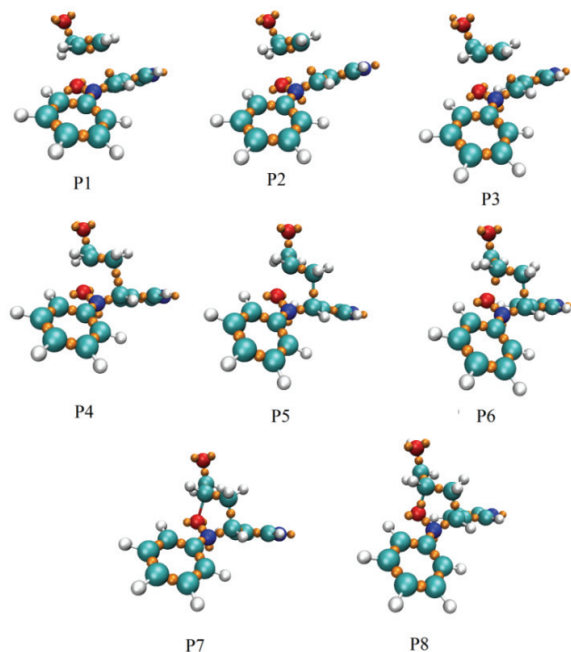


Fig. 6. Basin attractor positions of the points P1 to P8 along the exo/ortho pathway for 32CA reaction between 1 and 2; attractors are shown as spheres between the bonds s.

2. Point P1 with  $d_{C4-O1} = 2.34 \text{ \AA}$  and  $d_{C3-C5} = 2.44 \text{ \AA}$ , shows the generation of monosynaptic V(C3) basin integrating at basin population 0.17e, which derives its electron density from the disynaptic V(C3,N2) basin. V(C3) basin can be associated with the formation of pseudoradical centre at C3.

3. Point P2 with  $d_{C4-O1} = 2.30 \text{ \AA}$  and  $d_{C3-C5} = 2.37 \text{ \AA}$  is associated with the formation of monosynaptic V(N2) basin integrating at basin population 0.72e, which can be associated with the formation of N2 lone pair.

4. At Point P3 with  $d_{C4-O1} = 2.26 \text{ \AA}$  and  $d_{C3-C5} = 2.32 \text{ \AA}$ , the two disynaptic V(C4,C5) and V(C4,C5) are not visible, instead one single disynaptic V(C4,C5) basin integrating at basin population 3.20e is shown. This point is thus associated with the rupture of C4–C5 olefinic bond and requires 16.1 kcal mol<sup>-1</sup> energy. This supports the observation of Domingo *et al.*<sup>16</sup> that non-polar 32CAs show high activation energies and occur due to the rupture of olefinic C–C bonds, unlike polar processes where GEDT diminishes the activation energy barrier by depopulation of the olefinic double bond.

5. Point P4 with  $d_{C4-O1} = 2.14 \text{ \AA}$  and  $d_{C3-C5} = 2.15 \text{ \AA}$  is associated with the formation of monosynaptic V(C5) basin integrating at basin population 0.27e

can be associated with the formation of pseudoradical centre at C5, which derives electron density from the disynaptic V(C4,C5) basin, thereby drastically decreasing its electron density from 3.14e to 2.87e at P4. **TSox** belong to the same phase as P4, which indicates that C–C and C–O bond formation has not yet begun at **TSox**, that is also evident from the forming bond lengths (see Fig. 4) at the optimized transition state geometry.

6. Point P5 with  $d_{\text{C}4-\text{O}1} = 1.99 \text{ \AA}$  and  $d_{\text{C}3-\text{C}5} = 1.93 \text{ \AA}$  is associated with the formation of disynaptic V(C3,C5) basin integrating at basin population 1.28e, which can be associated with the formation of C3–C5 bond.

7. Point P6 with  $d_{\text{C}4-\text{O}1} = 1.98 \text{ \AA}$  and  $d_{\text{C}3-\text{C}5} = 1.91 \text{ \AA}$  is associated with the formation of monosynaptic V(C4) basin integrating at basin population 0.13e can be associated with the formation of pseudoradical centre at C4, which derives electron density from the disynaptic V(C4,C5) basin, thereby decreasing its electron density from 2.54e to 2.40e.

8. At P7, with  $d_{\text{C}4-\text{O}1} = 1.79 \text{ \AA}$  and  $d_{\text{C}3-\text{C}5} = 1.71 \text{ \AA}$ , the monosynaptic V(C4) basin is no longer visible, instead, there is abrupt increase in the V(O1)+ +V'(O1) basin population (see Fig. 5).

9. Point P8 with  $d_{\text{C}4-\text{O}1} = 1.74 \text{ \AA}$  and  $d_{\text{C}3-\text{C}5} = 1.67 \text{ \AA}$  shows the formation of disynaptic V(C4,O1) basin integrating at basin population 0.69e, which can be associated with the formation of C4–O1 bond.

Fig. 7 shows the ELF localization domains at the optimized transition states.

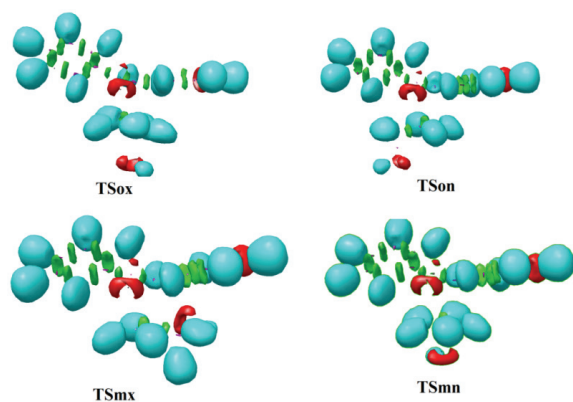


Fig. 7. B3LYP/6-311G(d,p) calculated ELF localization domains (iso-value: 0.86) at the transition states.

#### *Identification of interactions at the inter-atomic bonding regions by QTAIM & NCI studies*

Baden<sup>25</sup> proposed that atomic interactions present in molecular systems can be identified, assessed, and characterized by the gradient  $\nabla\rho_{(\mathbf{r})}$  and the Laplacian  $\nabla^2\rho_{(\mathbf{r})}$  of their electronic distribution. Classification of the interaction between a pair of bonded atoms was established by Bader and Esser<sup>26</sup> in 1984. QTAIM

parameters of (3,-1) bond critical points at the transition states in the regions associated with generation of new C-C and C-O single bonds are listed in Table III.

TABLE III. QTAIM parameters of (3,-1) critical points in the regions associated with generation of new C-C and C-O single bonds

TS	CP1 (C3-C5)			CP2 (C4-O1)		
	$\rho_{rc}$ / au	Laplacian of electron density, au	Energy density, au	$\rho_{rc}$ / au	Laplacian of electron density, au	Energy density, au
<b>TSox</b>	0.065	0.032	-0.016	0.055	0.114	-0.004
<b>TSon</b>	0.068	0.030	-0.017	0.051	0.108	-0.004
<b>TSmx</b>	0.065	0.029	-0.016	0.061	0.125	-0.006
<b>TSmn</b>	0.067	0.031	-0.015	0.060	0.123	-0.005

In each of the TSs, the Laplacian  $\nabla^2\rho_{(r)}$  shows positive value, which indicates non-covalent interaction at the interatomic bonding region. This is in complete agreement with the ELF topological study, which suggests that no bond formation has begun at the transition state **TSox**. The contour line maps of the Laplacian  $\nabla^2\rho_{(r)}$  along the ortho/exo pathway at the representative IRC points of different ELF topological phases are shown in Fig. 8. Earlier C3–C5 bond formation is predicted at P5, which agrees well with the ELF study showing the form-

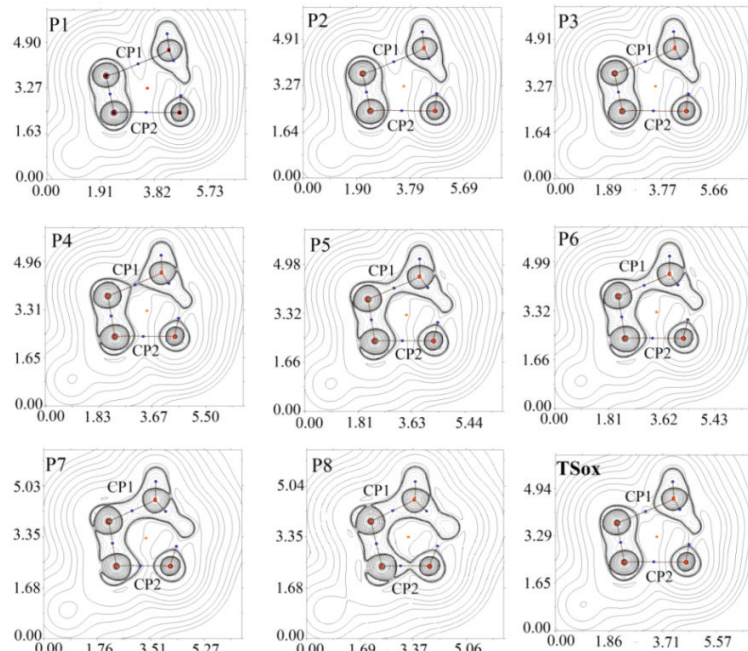


Fig. 8. Representations of the contour line maps of the Laplacian of the electron density along exo/ortho pathway of 32CA between **1** and **2** on the molecular plane defined by atoms for C3–C5 (C–C) and C4–O1 (C–O) bond formation.

ation of disynaptic V(C3,C5) basin at P5. The formation of C4–O1 bond takes place at P8, which is also in complete agreement with the ELF topological analysis.

NCI plot<sup>27</sup> is an approach based on the electron density and its derivatives to map and analyse bonding noncovalent interactions in molecular systems. Large negative values of sign  $(\lambda_2)\rho$  indicate attractive interactions such as dipole-dipole or hydrogen bonding, while large positive values of sign  $(\lambda_2)\rho$  indicate that the interaction is nonbonding. Weak, van der Waals interactions are indicated by near zero values of sign  $(\lambda_2)\rho$ . NCI gradient isosurfaces at the transition states are shown in Fig. 9. The C4–O1 and C3–C5 bonding regions show red and blue portions corresponding to the non-covalent interactions present at the interatomic bonding regions. The visibility of non-covalent attractive overlap at these regions is in complete agreement with the calculated QTAIM parameters and also agrees well with the GEDT & CDFT predictions suggesting non-polar character of this 32CA reaction.

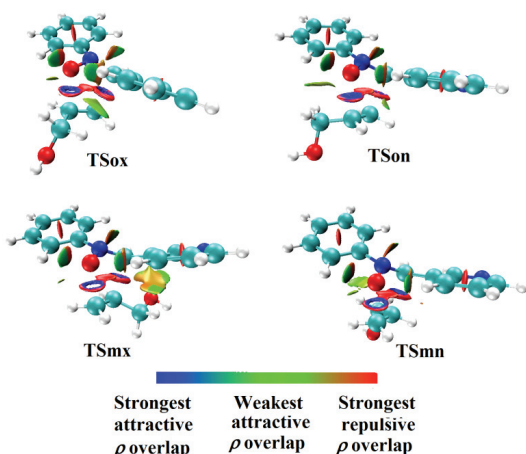


Fig. 9. NCI gradient isosurfaces of reduced density gradient (as values of sign  $(\lambda_2)\rho$ ) at the TSs. Surfaces are shown in  $(-0.04, 0.02$  scale) a.u. (isosurfaces = 0.5 a.u.).

## CONCLUSIONS

[3+2] cycloaddition reaction of *C*-(pyridin-3-yl)-*N*-phenyl nitrone to 2-propen-1-ol is regio- and stereoselective with the lowest activation energy barrier calculated for ortho/exo reaction pathway. This is in conformity with the experimental findings. The global electron density transfer and minimal difference in electronic chemical potentials of the reactants predict non-polar character of the reaction. One-step mechanism with asynchronous transition state is predicted. Topological analysis of the ELF along the IRC pathway shows coupling of pseudoradical centers to form new C–C and C–O bonds, with the faster C–C bond formation in agreement with the calculated QTAIM parameters and non-

-covalent interaction (NCI) plot of the transition states. Early transition states involving no C–C or C–O bond formation are predicted along each approach mode of this cycloaddition.

#### SUPPLEMENTARY MATERIAL

Optimized geometries and total energies of the reactants, products and transition states are available electronically at the pages of journal website: <http://www.shd.org.rs/JSCS/>, or from the corresponding author on request.

*Acknowledgement.* The author acknowledges the kind cooperation of Professor Manas Banerjee, Retired Professor of The University of Burdwan, West Bengal, India.

#### ИЗВОД

РАЗУМЕВАЊЕ РЕГИО И ДИЈАСТЕРЕОСЕЛЕКТИВНЕ СИНТЕЗЕ  
ИЗОКСАЗОЛИДИНСКОГ МОЋНОГ БЛОКАТОРА БОЛА ИЗ С-(ПИРИДИН-3-ИЛ)-Н-  
-ФЕНИЛНИТРОНА У СВЕТЛУ ТЕОРИЈЕ МОЛЕКУЛСКЕ ЕЛЕКТРОНСКЕ ГУСТИНЕ

NIVEDITA ACHARJEE

*Department of Chemistry, Durgapur Government College, J.N. Avenue, Durgapur, West Bengal, India*

Циклоадициона реакција [3+2] С-(пиридин-3-ил)-N-фенил нитрона и 2-пропен-1-ола даје стереохемијски дефинисан изоксазолидински дериват који је моћан блокатор бола. За ову синтезу су урађена рачунарска квантна израчунавања (CQC) да би се предвидели поларни карактер, механизам и селективност у оквиру теорије молекулске електронске густине (MEDT). Тополошка анализа функције локализације електрона (ELF) класификује нитрон као zwitter-јонску (zw-) троатомску компоненту (ТАС) показујући одсуство ма каквог псевдорадикалског или карбеноидног центра. Проучавана су четири реакциона канала који одговарају могућим регио- стереоселективним путевима на DFT/ /B3LYP/6-311G(d,p) нивоу теорије. Реакција следи једностепени механизам са асинхроним прелазним стањима, а израчунате енергије активације се добро слажу са експерименталним подацима. Реакција се може поделити у девет ELF тополошких фаза са бржим формирањем С–С веза. Теорија глобалне електронске густине (GEDT) на фаворизованом прелазном стању и индекси концептуалне теорије функционала густине (CDFT) за основно стање реагенаса указују на неполарни карактер. Нековалентне интеракције су предвиђене анализом атома-у-молекулу (AIM) и графицима нековалентних интеракција (NCI) у прелазним стањима.

(Примљено 14. септембра, ревидирано 19. новембра, прихваћено 16. децембра 2019)

#### REFERENCES

1. M. A. Chiacchio, S. V. Giofrè, R. Romeo, G. Romeo, U. Chiacchio, *Curr. Org. Synth.* **13** (2016) 726 (<https://doi.org/10.2174/157017941266150914195807>)
2. R. C. F. Jones, *The Chemistry of Heterocyclic Compounds Synthetic Applications of 1,3-Dipolar Cycloaddition Chemistry Toward Heterocycles and Natural Products*, John Wiley & Sons, New York 2002, pp. 1–81 (<https://doi.org/10.1002/0471221902.ch1>)
3. L. R. Domingo, *Molecules* **21** (2016) 1319 (<https://doi.org/10.3390/molecules21101319>)
4. M. R. Gutiérrez, L. R. Domingo, *Eur. J. Org. Chem.* **2** (2019) 267 (<https://doi.org/10.1002/ejoc.201800916>)
5. L. R. Domingo, M. R. Gutiérrez, N. Acharjee, *Molecules* **24** (2019) 832 (<https://doi.org/10.3390/molecules24050832>)

6. L. R. Domingo, M. R. Gutiérrez, P. Pérez, *J. Org. Chem.* **83** (2018) 2182 (<https://doi.org/10.1021/acs.joc.7b03093>)
7. D. Hallooman, D. Cudian, M. R. Gutiérrez, L. Rhyman, I. A. Alswaidan, M. I. Elzagheid, L. R. Domingo, P. Ramasami, *ChemistrySelect* **2** (2017) 9736 (<https://doi.org/10.1002/slct.201702136>)
8. L. R. Domingo, M. R. Gutiérrez, P. Pérez, *Molecules* **23** (2018) 1913 (<https://doi.org/10.3390/molecules23081913>)
9. A. I. Adjieufack, I. M. Ndassa, J. K. Mbadcam, M. R. Gutiérrez, L. R. Domingo, *Theor. Chem. Acc.* **136** (2017) 129 (<https://doi.org/10.1007/s00214-017-2161-4>)
10. A. Kącka-Zych, R. Jasiński, *Theor. Chem. Acc.* **138** (2019) 81 (<https://doi.org/10.1007/s00214-019-2467-5>)
11. A. Kącka-Zych, *Molecules* **24** (2019) 462 (<https://doi.org/10.3390/molecules24030462>)
12. A. D. Becke, K. E. Edgecombe, *J. Chem. Phys.* **92** (1990) 5397 (<https://doi.org/10.1063/1.458517>)
13. L. R. Domingo, M. R. Gutiérrez, P. Pérez, *Molecules* **21** (2016) 748 (<https://doi.org/10.3390/molecules21060748>)
14. B. Silvi, A. Savin, *Nature* **371** (1994) 683 (<https://www.nature.com/articles/371683a0>)
15. L. R. Domingo, M. R. Gutiérrez, P. Pérez, *Tetrahedron* **72** (2016) 1524 (<https://doi.org/10.1016/j.tet.2016.01.061>)
16. L. R. Domingo, M. R. Gutiérrez, *Molecules* **22** (2017) 750 (<https://doi.org/10.3390/molecules22050750>)
17. L. R. Domingo, N. Acharjee, *ChemistrySelect* **3** (2018) 8373 (<https://doi.org/10.1002/slct.201801528>)
18. L. R. Domingo, *RSC Adv.* **4** (2014) 32415 (<https://doi.org/10.1039/C4RA04280H>)
19. A. E. Reed, R. B. Weinstock, F. Weinhold, *J. Chem. Phys.* **83** (1985) 735 (<https://doi.org/10.1063/1.449486>)
20. A. E. Reed, L. A. Curtiss, F. Weinhold, *Chem. Rev.* **88** (1985) 899 (<https://doi.org/10.1021/cr00088a005>)
21. L. R. Domingo, M. R. Gutiérrez, P. Pérez, *Tetrahedron* **73** (2017) 1718 (<https://doi.org/10.1016/j.tet.2017.02.012>)
22. C. González, H. B. Schlegel, *J. Phys. Chem.* **94** (1990) 5523 (<https://doi.org/10.1021/j100377a021>)
23. J. Andrés, S. Berski, L. R. Domingo, V. Polo, B. Silvi, *Curr. Org. Chem.* **15** (2011) 3566 (<https://doi.org/10.2174/13852721179763156>)
24. J. Andrés, S. Berski, B. Silvi, *Chem. Commun.* **52** (2016) 8183 (<https://doi.org/10.1039/C5CC09816E>)
25. R. F. W. Bader, In *Atoms in Molecules: A Quantum Theory*, Clarendon Press, Oxford, 1990
26. R. F. W. Bader, H. Essén, *J. Chem. Phys.* **80** (1984) 1943 (<https://doi.org/10.1063/1.446956>)
27. J. C. García, E. R. Johnson, S. Keinan, R. Chaudret, J. P. Piquemal, D. N. Beratan, W. Yang, *J. Chem. Theory Comput.* **73** (2011) 625 (<https://doi.org/10.1021/ct100641a>)
28. N. Sethi, R. Bhatti, M. P. S. Ishar, *Res. Pharm. Sci.* **9** (2014) 59 (<https://www.ncbi.nlm.nih.gov/pmc/articles/PMC4292182>)
29. A. D. Becke, *Phys. Rev., A* **38**(1988) 3098 (<https://doi.org/10.1103/PhysRevA.38.3098>)
30. C. Lee, W. Yang, R. G. Parr, *Phys. Rev., B* **37** (1988) 785 (<https://doi.org/10.1103/PhysRevB.37.785>)

31. P. Geerlings, F. De. Proft, W. Langenaeker, *Chem. Rev.* **103** (2003) 1793 (<https://doi.org/10.1021/cr990029p>)
32. R. G. Parr, W. Yang, *Density Functional Theory of Atoms and Molecules*, Oxford University Press, New York, 1989
33. R. G. Parr, R. G. Pearson, *J. Am. Chem. Soc.* **105** (1983) 7512 (<https://doi.org/10.1021/ja00364a005>)
34. L. R. Domingo, M. J. Aurell, P. Pérez, R. Contreras, *Tetrahedron* **58** (2002) 4417 ([https://doi.org/10.1016/S0040-4020\(02\)00410-6](https://doi.org/10.1016/S0040-4020(02)00410-6))
35. L. R. Domingo, P. Pérez, *Org. Biomol. Chem.* **9** (2011) 7168 (<https://doi.org/10.1039/C1OB05856H>)
36. J. Tomasi, M. Persico, *Chem. Rev.* **94** (1994) 2027 (<https://doi.org/10.1021/cr00031a013>)
37. M. Cossi, V. Barone, R. Cammi, J. Tomasi, *Chem. Phys. Lett.* **255** (1996) 327 ([https://doi.org/10.1016/0009-2614\(96\)00349-1](https://doi.org/10.1016/0009-2614(96)00349-1))
38. *Gaussian 03, Revision D.01*, Gaussian, Inc., Wallingford, CT, 2004
39. T. Lu, F. Chen, *J. Comp. Chem.* **33** (2012) 580 (<https://doi.org/10.1002/jcc.22885>)
40. W. Humphrey, A. Dalke, K. Schulten, *J. Mol. Graphics* **14** (1996) 33 ([https://doi.org/10.1016/0263-7855\(96\)00018-5](https://doi.org/10.1016/0263-7855(96)00018-5))
41. E. F. Pettersen, T. D. Goddard, C. C. Huang, G. S. Couch, D. M. Greenblatt, E. C. Meng, T. E. Ferrin, *J. Comput. Chem.* **25** (2004) 1605 (<https://doi.org/10.1002/jcc.20084>)
42. E. Dresler, A. Kącka-Zych, M. Kwiatkowska, R. Jasiński, *J. Mol. Model.* **24** (2018) 329 (<https://doi.org/10.1007/s00894-018-3861-y>)
43. R. Jasiński, *Comput. Theor. Chem.* **1125** (2018) 77 (<https://doi.org/10.1016/j.comptc.2018.01.009>)
44. R. Jasiński, *Tetrahedron Lett.* **56** (2015) 532 (<https://doi.org/10.1016/j.tetlet.2014.12.007>)
45. R. Jasiński, M. Żmigrodzka, E. Dresler, K. Kula, *J. Heterocyclic. Chem.* **54** (2017) 3314 (<https://doi.org/10.1002/jhet.2951>)
46. R. Jasiński, K. Mróz, A. Kącka, *J. Heterocycl. Chem.* **53** (2016) 1424 (<https://doi.org/10.1002/jhet.2442>).